NUMERICAL INVESTIGATION OF THE NEAR-FIELD FLOW-STRUCTURES PRODUCED BY A PITCHED AND SKEWED VORTEX GENERATING JET

James W. Jewkes
Fluid Dynamics Research Group,
Curtin University of Technology,
Perth, W.A. 6845, Australia
J.Jewkes@Curtin.edu.au

Yongmann M. Chung
School of Engineering, and Centre for Scientific Computing
University of Warwick,
Coventry, CV4 7AL, U.K.
Y.M.Chung@warwick.ac.uk

ABSTRACT

A large-eddy simulation of a velocity-ratio ($VR = 1.0$), pitched and skewed vortex generating jet issuing into a turbulent boundary layer ($Re_{\delta^*} = 2000$) is presented. As the jet issues from the orifice, an asymmetrical counter-rotating vortex pair is produced, consisting of a strong primary vortex and a weaker secondary vortex. The secondary vortex quickly dissipates to leave the primary vortex, which persists farther downstream. The primary vortex replaces the near-wall region with higher momentum fluid, and is shown to be associated with improved skin friction downstream of the jet. This increase in skin friction has been previously shown to be associated with improved resistance to boundary-layer separation.

INTRODUCTION

The flow-field associated with a steady jet issuing perpendicular to a flat plate turbulent boundary layer (TBL) is a 'kernel' fluid dynamics configuration. A parameter often used to characterise a jet in cross flow (JICF) is the velocity ratio, $VR = U_j/U_\infty$, the ratio between the average velocity of the steady jet (U_j) and the free-stream (U_∞). Another useful parameter is the relationship between the jet diameter and the boundary-layer thickness (D/δ). Our interest in the JICF stems from its potential application in boundary-layer flow separation control (in this context, they are usually described as vortex generating jets (VGJs)). These devices produce streamwise 'corkscrew' vortices, which transport fluid from the high-momentum free-stream into the low-momentum near-wall region. For flow separation control, it is desirable to enhance momentum *within* the TBL, since an energised boundary layer is less prone to flow separation (Johnston (1999)). Many of the previous perpendicular jet investigations have been concerned with the behaviour of high velocity-ratio jets (typically $VR > 2$, *e.g.*, Yuan *et al.* (1999)) or with jets much larger than the boundary layer thickness (*e.g.*, Andreopoulos & Rodi (1984)). High velocity-ratio perpendicular jets have a tendency to project away from the wall, through the boundary-layer and into the free-stream and they are not particularly useful for separation control applications.

Early work by Wallis (1960) indicated that a pitched and skewed jet configuration has a far more favourable effect on flow separation than a perpendicular jet. His aerofoil experiments set a precedent of pitching the jet by $\beta = 45^\circ$ and skewing it by $\alpha = 90^\circ$ relative to the boundary layer. The experimental work of Johnston and his colleagues (Johnston & Nishi (1990); Compton & Johnston (1992); Johnston (1999); Khan & Johnston (2000)) explained more about the structure of the pitched and skewed jet. It is well known that perpendicular jets produce a symmetrical counter-rotating vortex pair, consisting of two equally sized vortices (Margason (1993); Fric & Roshko (1994)). Khan & Johnston (2000) established that a pitched and skewed jet initially forms an asymmetric counter-rotating vortex pair (CVP) comprised of a stronger primary vortex, and a weaker secondary vortex, which quickly dissipates. It is believed that the increased residual momentum in the primary vortex causes it to persist farther downstream, and is key to the pitched and skewed jet's improved ability to delay flow separation compared to the perpendicular jet case. The recent VGJ research, AeroMEMS II project (Warsop (2004, 2006)), has focused on pitched and skewed pulsating jets, which have been shown to be even more effective for boundary-layer flow separation control (Godard & Stanislas (2006*b*); Warsop & Hucker (2007); Laval *et al.* (2010)). Both experimental and numerical work (Godard & Stanislas (2006*a*); Godard *et al.* (2006); Godard & Stanislas (2006*b*); Laval *et al.* (2010)) has made a significant contribution to the parameterisation of the effect of various configurations of steady and pulsating VGJ on flow separation. However, whilst the parameterisation has been exhaustive, there still remain gaps in our understanding of the evolution of these pitched and skewed VGJs. So far, the best description of the near-field has been produced by Zhang & Collins (1997), however the intrinsic limitations of experimental measurement techniques have meant that some key structures have been inferred rather than fully described, and other structures have been overlooked.

In this paper we explore in detail the near-field evolution of structures in the pitched and skewed jet configuration; a steady jet with the pitch angle $\beta = 45^\circ$ and the skew angle $\alpha = 90^\circ$ is considered. This work is an extension of our previous work on TBL simulation (Jewkes *et al.* (2011)), where a variant of the Lund *et al.* (1998) inflow generation method was developed and validated well against DNS data.

While early VGJ research has mainly been conducted experimentally, computer simulations have recently also been utilised. As noted by Johnston (1999), initial attempts at CFD simulations of VGJs (*e.g.*, Henry & Pearcey (1994)), were performed using Reynolds-Averaged Navier-Stokes solvers, and near-field agreement with experimental data was generally poor. More recently, large-eddy simulation (LES) and direct numerical simulation (DNS) have enabled researchers to resolve instantaneous structures, and produce simulations that demonstrate excellent agreement with experimental data (*e.g.*, Yuan *et al.* (1999); Muppidi & Mahesh (2007); Selent & Rist (2010); Laval *et al.* (2010)). Despite the technological advancements, TBL separation control simulations remain problematic. In LES and DNS, downstream flow is particularly sensitive to the inlet boundary condition, and with TBLs it is essential to provide a realistic, coherent series of instantaneous, time-varying velocity components to avoid spurious, non-physical behavior (Jewkes *et al.* (2011)). This issue has often been circumvented by performing simulations of a jet interacting with a laminar boundary layer (*e.g.*, Yuan *et al.* (1999); Muppidi & Mahesh (2007); Selent & Rist (2010)). However, this is an undesirable assumption in the context of flow separation control since the mechanism of these devices relies on increasing the turbulence in the boundary layer itself. The parameterisation work of Laval *et al.* (2010) represents perhaps the most sophisticated and accurate series of separation control simulations to date. Their approach was to use a turbulent channel flow based model that included a wall-mounted hump.

Numerical Formulation

Results have been computed using a second-order finite-volume large eddy simulation code (Chung (2005); Chung & Talha (2011); Jewkes *et al.* (2011)). The convective terms were modelled using a third order Runge-Kutta method, and the diffusive terms using a Crank-Nicolson method. A fractional-step time-advancement was used and a dynamic subgrid-scale model was applied to calculate the Smagorinsky constant. Length scales were non-dimensionalised with respect to the inlet displacement thickness, δ^*_{inlt}, and velocities with respect to the free-stream velocity, U_∞. The resulting Re number is defined as $Re_{\delta^*} = \frac{U_\infty \delta^*}{\nu} = 2000$ at the inlet, where ν is the kinematic viscosity. The simulation domain had dimensions $128\delta^* \times 32\delta^* \times 4\pi\delta^*$ in streamwise (x), wall normal (y) and spanwise (z) directions. Grid resolutions were $200 \times 60 \times 96$ points, yielding $\Delta x^+ = 59$, $\Delta y^+_{wall} \approx 1.2$, and $\Delta z^+ = 18$, uniform in x and z, and applying hyperbolic tangent stretching in the wall-normal direction. Inlet boundary conditions were provided by a precursor simulation based on a variant of the Lund *et al.* (1998) formulation, as described in Jewkes *et al.* (2011). Upper boundary conditions were $u = U_\infty$, $\frac{\partial v}{\partial y} = 0$, $\frac{\partial w}{\partial y} = 0$, the spanwise domain boundary was periodic, and the exit plane used a convective boundary condition. Further details can be found in Jewkes *et al.* (2011).

The origin of our coordinate system was located at the centre of the jet orifice. The $VR = 1$ jet was located on the spanwise centreline, $x_{jet} = 48\delta^* \approx 6\delta$ downstream of the domain inlet, (37.5% of the streamwise domain length, corresponding to $Re_\theta \approx 1650$ in the flat plate case), with a circular orifice of diameter $D = 4\delta^* \approx 0.5\delta$. This configuration compares well with many of the existing separation control oriented VGJ studies. Jet velocity boundary conditions were applied at the wall, the profile provided by a hyperbolic tangent function (Chung *et al.* (2002)). It is worth noting that detailed information on the jet profile is not usually available in experiments. The effect of the jet profile on the early jet development can be found in Kim & Choi (2009).

Results and Discussion

First, an LES of a TBL without a jet was performed for $Re_{\delta^*} = 2000$, and the results were compared with available DNS (Spalart (1988)) and LES (Lund *et al.* (1998)) data at similar Re numbers. The mean velocity and rms velocity fluctuation profiles showed very good agreement, demonstrating that our inflow generation method (Jewkes *et al.* (2011)) is effective in this type of TBL study.

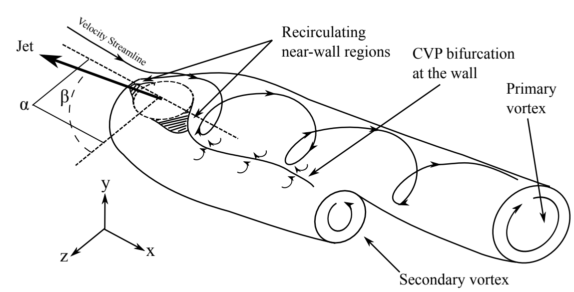

Figure 1. Sketch illustrating key structures in the $VR = 1$ pitched ($\beta = 45^\circ$) and skewed ($\alpha = 90^\circ$) jet flow-field.

Next, a pitched and skewed jet case is considered. The jet velocity boundary condition was modified, such that the jet was pitched by $\beta = 45^\circ$ to the wall, and then skewed by $\alpha = 90^\circ$ relative to the free-stream. This pitch and skew configuration dates back to the early experimental work of Wallis (1960), and is consistent with later work (Johnston & Nishi (1990); Compton & Johnston (1992); Zhang & Collins (1997)). Among others, the experimental work of Zhang & Collins (1997) is particularly interesting, being broadly similar in configuration to our model, and being one of the few papers concerned specifically with the evolution of structures in the near-field. Comparisons are made between the present results and Zhang & Collins (1997).

Figure 1 shows an illustration of the configuration of our low-*VR* pitched and skewed jet flow-field. Key structures observable in our data include the primary and secondary vortices, recirculating near-wall regions, and a counter-rotating vortex pair (CVP) bifurcation line at the wall.

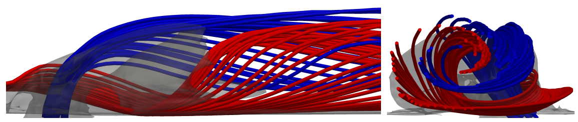

(a) (b)

Figure 2. The $VR = 1$ pitched ($\beta = 45^\circ$) and skewed ($\alpha = 90^\circ$) jet. a) xy view. (The flow direction is from left to right); b) yz view. (The flow direction is out of the paper).

Figure 2 shows 3D views of the time-averaged structures near the jet, in the z and x axes respectively. Red velocity streamlines are seeded from a line placed just in front of the jet ($y/D = 0.6$, $x/D = -1$), blue velocity streamlines issue from the jet orifice, the isosurface represents a vorticity magnitude of $|\omega| = 0.5$. The largest and most recognisable structure within the pitched and skewed jet flow-field is the primary vortex. Figure 2 shows upstream boundary-layer fluid passing over the jet near the jet exit, and sweeping underneath into the primary vortex; it indicates how the slow-moving near-wall boundary layer fluid downstream of the jet is replaced with fluid from outer, higher momentum regions of the boundary layer.

Figure 3 shows normalised (v, w) velocity vectors (coloured by velocity magnitude) in yz planes to give a clearer impression of the near-field rotation induced by the jet. Counter-rotating vortices are clearly seen at $x/D = 1$; the primary vortex is located further away from the wall, compared to the secondary vortex. The development of a counter-rotating vortex pair (CVP) is well documented for the high *VR* perpendicular jet configuration (*e.g.*, Fric & Roshko (1994)), the CVP comprising of two equally sized vortices which advect downstream; the evolution of the pitched and skewed case bears some similarity. Moving downstream to $x/D = 2$, the CVP origins of the primary vortex are still clearly seen in Figure 3b; the primary vortex located at $z/D = 0.4$, $y/D = 0.5$, and a weaker secondary vortex located at $z/D = 1.4$, $y/D = 0.3$, this is consistent with the positive and negative regions of vorticity (not shown here). These vortices move in the positive spanwise direction as they travel further downstream. The primary vortex moves also away from the wall as it travels downstream, while no such wall normal movement is observed in the secondary vortex. An ejection of low momentum fluid is observed between the two vortices while a sweep of the high momentum fluid occurs on the opposite sides of the vortices. The secondary vortex is dissipated further downstream at $x/D = 4$, and only the primary vortex remains in Figure 3c. The vorticity plot (not shown here) shows a region of strong vorticity at the centre of the vortex($z/D = 0.7$, $y/D = 0.7$). This single counter-clockwise streamwise vortex moves fluid away from the wall at $z/D = 1$, and toward the wall at $z/D = 0$, resulting in a thickening of the near-wall boundary layer on the upwash side of the vortex, and a thinning on the downwash side.

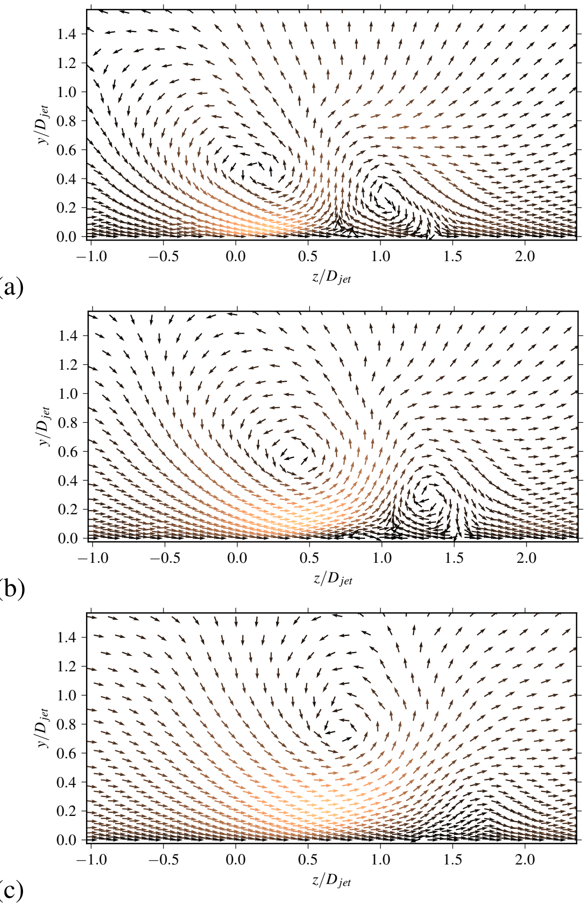

(a) (b) (c)

Figure 3. Normalised vector plot of time-averaged (v, w) velocity in yz planes. Vectors are coloured by velocity magnitude. a) $x/D = 1$, b) $x/D = 2$, c) $x/D = 4$. Velocity fields are interpolated into a uniform grid to improve the clarity of vector plot.

Figure 4 shows the development of u velocity in the near-field downstream of the jet. In Figure 4a, located just downstream of the jet orifice ($x/D = 1$), boundary layer thinning is clearly seen at around $z/D = -0.3$ and $z/D = 1.2$ due to the sweeping of the primary and the secondary vortices. A thickening of the boundary layer is observed in between; C_f has a local minimum at $z/D = 0.4$. There are lobes of low velocity located at $x/D = 0.25$, $y/D = 0.5$ and $x/D = 0.75$, $y/D = 0.5$, near the centres of the counter-rotating vortices shown in Figure 3. Figures 4b and 4c show that this streamwise momentum deficit decreases as the vortices move downstream while its location is convecting in the positive spanwise direction. As suggested by Khan & Johnston (2000), a streamwise velocity deficit in this region is a result of the movement of low-speed boundary-layer fluid into the core. In Figure 4c, it is clearly seen that the single streamwise vortex affects the TBL significantly at $x/D = 4$; the boundary layer thickens around $z/D = 1$, and thins around $z/D = 0$.

As the near-wall flow resolves itself between the counter-

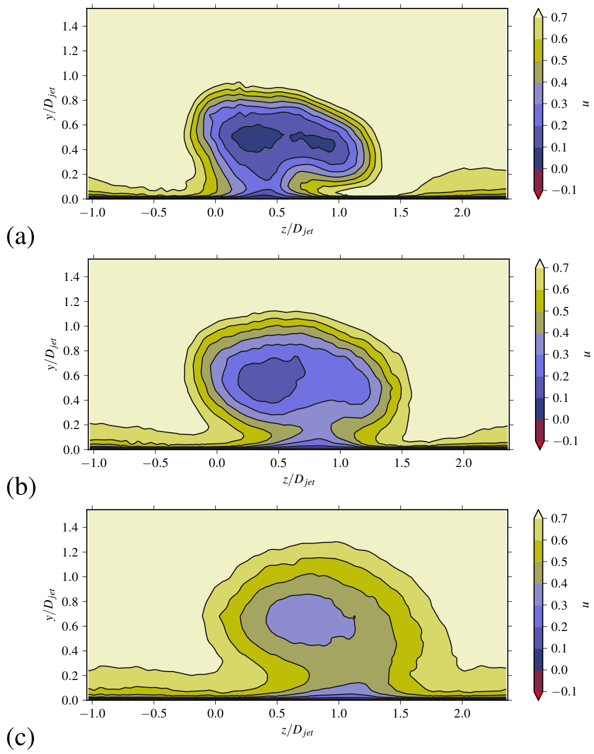

Figure 4. yz planes showing time-averaged u velocity; a) $x/D = 1$, b) $x/D = 2$, c) $x/D = 4$.

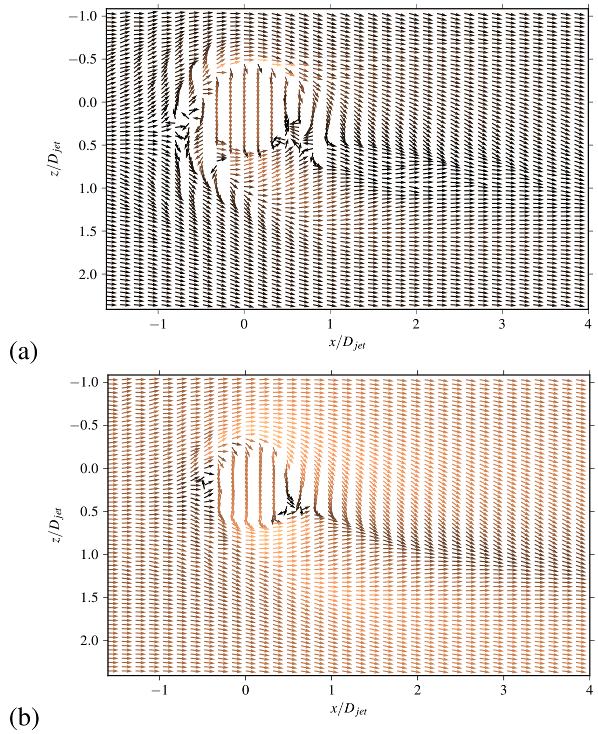

Figure 5. Normalised vector plot of time-averaged (u, w) velocity in xz planes. Vectors are coloured by magnitude. a) $y/D = 0$ (wall), b) $y/D = 0.3$.

rotating vortex pair, a bifurcation line lies between the two vortices. Normalised vector plot in $x-z$ plane shown in Figure 5 highlights this bifurcation line. The bifurcation line was first observed in surface oil-flow visualisations by Zhang & Collins (1997). The region between $z/D = -0.7$ to $z/D = 0.7$ further downstream of the jet shows the boundary-layer flow being swept in a spanwise direction into the primary vortex.

Figure 6a shows time-averaged u velocity profiles at several z locations across the $x/D = 4$ plane (and also shown is the original flat-plate TBL velocity profile from Jewkes *et al.* (2011)). It is found that the downwash side of the vortex ($z/D = 0$) has fuller streamwise velocity profiles than upwash side of the vortex ($z/D = 1$). The skin friction (C_f) plot in Figure 6 shows that this leads to increased wall shear-stress on the downwash side of the vortex for $x/D > 0.5$, relative to an unperturbed flat-plate TBL. Initially, skin friction is strong at $z/D = -0.5$, $-2 < x/D < 3$, and at $z/D = 1$ (representing the acceleration of near-wall flow around the blockage of the jet) . For $3 < x/D < 8$, $z/D = 0$ shows high skin friction, moving to $z/D = 0.5$ for $8 < x/D < 12$, and $z/D = 1$ for $x/D > 12$. The effect of vortical structures on the wall shear stress is observed to track the spanwise advection of the primary vortex, and increased C_f persists far downstream. This increase in skin friction lies at the heart of the VGJ's ability to delay stall and separation Laval *et al.* (2010).

Figure 7a shows the streamwise u velocity. The flow immediately downstream of the jet is characterised by a near-wall region of recirculating flow. Figure 7a clearly shows that this negative u velocity lies in the near-wall, starting at the side of the jet ($x/D = -0.5$, $z/D = 0.4$), moving round the back of the jet to $x/D = 0.5$, $z/D = 0.5$, and extending downstream to $x/D = 1$. The velocity vector plot (Figure 5) shows that within this region there is reverse-flow that appears to sweep from the negative z side of the jet to the positive, recirculating immediately behind the jet column. Again, Figure 5b shows that this recirculation extends at least $y/D = 0.1$ away from the wall, and Figure 7b (a yz plane, located immediately downstream of the jet orifice, $x/D = 0.5$) indicates that it may in fact reach $y/D = 0.2$. Time-averaged skin friction (Figure 6b) shows that there is again a very clear region of negative skin friction downstream of the jet at $z/D = 0.5$. This recirculation is not shown by Zhang & Collins (1997)'s oil-flow plots. However, his velocity vectors (at $y/D = 0.07$) show a 'spiral point' at approximately $x/D = 1$, which can be seen in Figure 5a. This 'spiral' point corresponds with the recirculating region resolving itself into the counter-rotating vortex pair bifurcation line.

There is a similar region of recirculating flow upstream of the jet. Figure 5a indicates that another recirculating region is located upstream of the jet. The u velocity plot (Figure 7a) shows that reverse-flow extends from $z/D = 0$ to $z/D = 1$ in the spanwise direction, and as far as $x/D = -0.9$ upstream of the jet. The vectors in Figure 5a show that within this region ($z/D = 0.2$ to $z/D = 0.8$), the flow is oriented upstream in the positive z direction. Figure 5b shows that this upstream recirculation extends at least $y/D = 0.1$ away from the wall, and Figure 8a (located at the upstream edge of the jet orifice, $x/D = -0.5$) indicates that it may reach $y/D = 0.2$. In Figure 6b, there is a very clear region of negative skin friction upstream (at $z/D = 0.5$) of the jet.

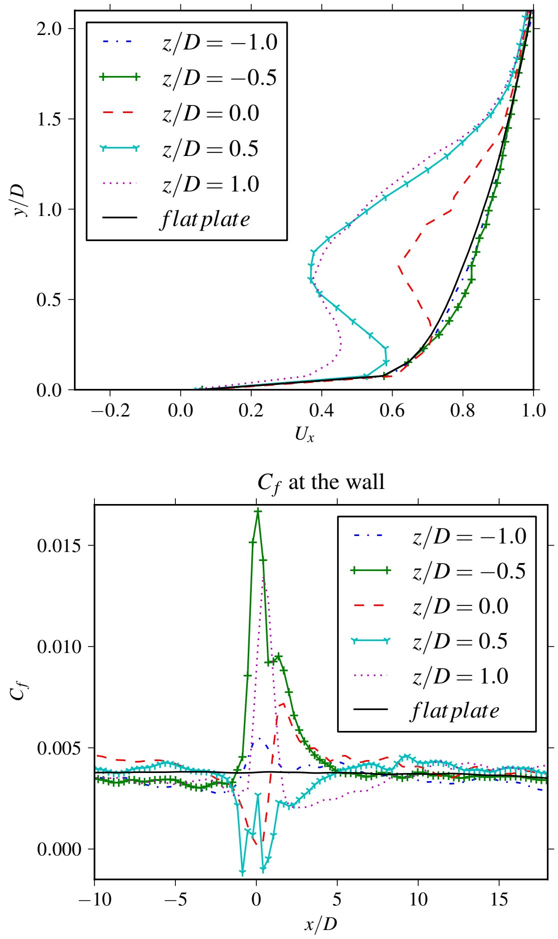

Figure 6. a) Time-averaged u velocity profiles across the wake of the jet, at $x/D = 4$, b) Skin friction, C_f along the x axis.

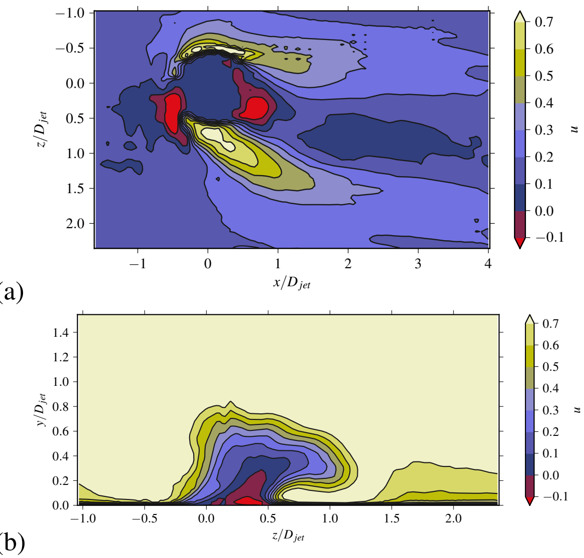

Figure 7. Planes showing time-averaged u velocity; a) xz plane, $y/D = 0$ (wall), b) yz plane, $x/D = 0.6$.

Zhang & Collins (1997) provided surface oil-flow plots which indicate similar behaviour, however their LDA measurements made at $y/D = 0.07$ showed no evidence of reverse-flow, which led him to infer that it is confined to a region very close to the wall. Our data confirms this hypothesis, and we would argue that the weak reverse-flow in fact represents near-wall stagnation caused by the blockage of the jet.

Conclusions

These results represent the first LES pitched and skewed VGJ simulations to utilise an accurate boundary layer model (provided by Jewkes *et al.* (2011)). As the jet issues from the orifice, an asymmetrical counter-rotating vortex pair is produced, consisting of a strong primary vortex and a weaker secondary vortex. The secondary vortex quickly dissipates to leave the primary vortex, which persists farther downstream. The primary vortex sweeps fluid from the cross-flow boundary layer, which thickens on the upwash side of the vortex and thins on the downwash side. The primary vortex contains a core of slow-moving fluid from the boundary layer, the near-wall region replaced by higher momentum fluid. This increase in momentum is shown to be associated with improved skin friction downstream of the jet. The increase in skin friction has been previously shown to be associated with increased resistance to boundary-layer separation. This study has revealed the existence of a near-wall region of reverse-flow downstream of the jet orifice. This region of reverse-flow is resolved into a vortex pair bifurcation line at a 'spiral point' directly behind the jet. The bifurcation line persists downstream, between the vortex pair until the secondary vortex dissipates. In future studies, we would like to correlate the evolution of these near-field structures, the primary and secondary vortices, with the resulting effect on shear-stress downstream, for various configurations. Ultimately, we would like to explain why certain velocity ratios, jet orientations, (also pulsation frequencies and duty cycles) have been shown by authors such as Laval *et al.* (2010) to be more effective for flow separation control.

Acknowledgments

This work was supported by the Engineering and Physical Sciences Research Council through the UK Turbulence Consortium (Grant EP/G069581/1). It follows on from work funded as part of the European collaborative research project (AEROMEMS II) CEC 5th framework, Promoting Competitive and Sustainable Growth programme, Key Action 4 - New Perspectives in Aeronautics (contract G4RD-CT-2002-00748).

REFERENCES

Andreopoulos, J. & Rodi, W. 1984 Experimental investigation of jets in a crossflow. *Journal of Fluid Mechanics* **138**, 93–127.

Chung, Y. M. 2005 Unsteady turbulent flow with sudden pres-

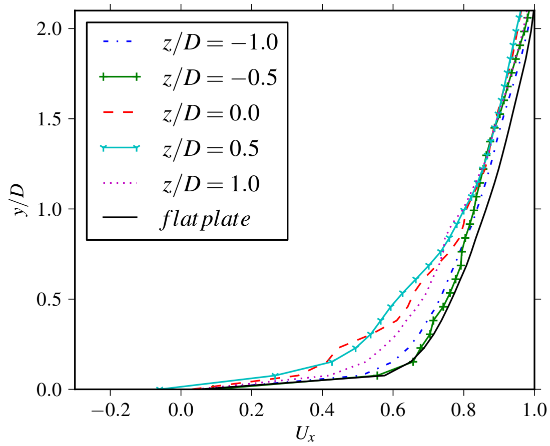

(a)

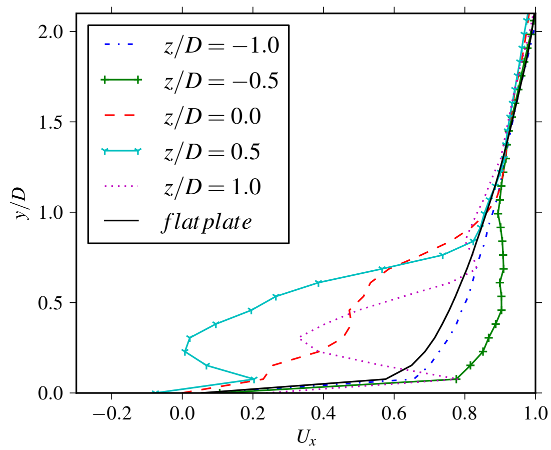

(b)

Figure 8. Time-averaged u velocity profiles across the jet, a) $x/D = -0.6$, b) $x/D = 0.6$

sure gradient changes. *International Jounal for Numerical Methods in Fluids* **47**, 925–930.

Chung, Y. M., Luo, K. H. & Sandham, N. D. 2002 Numerical study of momentum and heat transfer in unsteady impinging jets. *International Journal of Heat and Fluid Flow* **23**, 592–600.

Chung, Y. M. & Talha, T. 2011 Effectiveness of active flow control for turbulent skin friction drag reduction. *Physics of Fluids* **23** (2), 025102.

Compton, D. A. & Johnston, J. P. 1992 Streamwise vortex production by pitched and skewed jets in a turbulent boundary layer. *AIAA Journal* **30** (3), 640–647.

Fric, T. F. & Roshko, A. 1994 Vortical structure in the wake of a transverse jet. *Journal of Fluid Mechanics* **279**, 1–47.

Godard, G., Focaut, J. M. & Stanislas, M. 2006 Control of a decelerating boundary layer. part 2: Optimization of slotted jets vortex generators. *Aerospace Science and Technology* **10**, 394–400.

Godard, G. & Stanislas, M. 2006*a* Control of a decelerating boundary layer. part 1: Optimization of passive vortex generators. *Aerospace Science and Technology* **10**, 181–191.

Godard, G. & Stanislas, M. 2006*b* Control of a decelerating boundary layer. part 3: Optimization of round jets vortex generators. *Aerospace Science and Technology* **10**, 455–464.

Henry, F. S. & Pearcey, H. H. 1994 Numerical model of boundary-layer control using air-jet generated vortices. *AIAA Journal* **32**, 2415–2425.

Jewkes, J. W., Chung, Y. M. & Carpenter, P. W. 2011 Modification to a turbulent inflow generation method for boundary layer flows. *AIAA Journal* **49** (1), 247–250.

Johnston, J. P. 1999 Pitched and skewed vortex generator jets for control of turbulent boundary layer separation: A review. In *Proceedings of the 3rd ASME/JSME Joint Fluids Engineering Conference*. 18-23 July, San Francisco, California.

Johnston, J. P. & Nishi, M. 1990 Vortex generator jets - means for flow separation control. *AIAA Journal* **28**, 989–994.

Khan, Z. U. & Johnston, J. P. 2000 On vortex generating jets. *International Journal of Heat and Fluid Flow* **21**, 506–511.

Kim, J. & Choi, H. 2009 Large eddy simulation of a circular jet: effect of inflow conditions on the near field. *Journal of Fluid Mechanics* **620**, 383–411.

Laval, J.-P., Braud, C., Fournier, G. & Stanislas, M. 2010 Large-eddy simulations of control of a separated flow over a 2d bump by means of pulsed jets. *Journal of Turbulence* **11** (52), 1–33.

Lund, T. S., Wu, X. & Squires, K. D. 1998 Generation of turbulent inflow data for spatially-developing boundary layer simulations. *Journal of Computational Physics* **140** (2), 233–258.

Margason, R. J. 1993 Fifty years of jet in cross-flow research. *Tech. Rep.*. AGARD, National Aeronautics and Space Administration. Ames Research Center, Moffett Field, CA.

Muppidi, S. & Mahesh, K. 2007 Direct numerical simulation of round turbulent jets in crossflow. *Journal of Fluid Mechanics* **574**, 59–84.

Selent, B. & Rist, U. 2010 *Direct numerical simulation of jet in crossflow actuators*, chap. 5, pp. 241–253. Springer.

Spalart, P. R. 1988 Direct simulation of a turbulent boundary layer up to $Re_\theta = 1410$. *Journal of Fluid Mechanics* **187**, 61–98.

Wallis, R. A. 1960 A preliminary note on a modified type of air jet for boundary layer control. *ARC Current Papers* **513**, 1–6.

Warsop, C. 2004 AEROMEMS-II - a European research effort to develop MEMS based flow control technologies.

Warsop, C. 2006 Results and lessons learned from the European AEROMEMS II project.

Warsop, C. & Hucker, M. 2007 Pulsed air-jet actuators for flow separation control. *Flow, Turbulence and Combustion* **78**, 255–281.

Yuan, L. L., Street, R. L. & Ferziger, J. H. 1999 Large-eddy eimulations of a round jet in crossflow. *Journal of Fluid Mechanics* **379**, 71–104.

Zhang, X. & Collins, M. W. 1997 Nearfield evolution of a longitudinal vortex generated by an inclined jet in a turbulent boundary layer. *ASME: Journal of Fluids Engineering* **119**, 934–939.